Electrochemistry Communications 140 (2022) 107332

Contents lists available at ScienceDirect

Electrochemistry Communications

journal homepage: www.elsevier.com/locate/elecom

Significant two-step potential-induced surface reconstruction observed on Au(1 1 1) in aqueous sulfuric acid

Joseph Hamill [a], Kazem Zhour [b], Diddo Diddens [c], Masoud Baghernejad [c,*]

[a] Department of Chemistry and Nano-Science Center, University of Copenhagen, Universitetsparken 5, DK-2100, Copenhagen Ø, Denmark
[b] Institute of Physical Chemistry, University of Münster, Corrensstraße 28/30, 48149 Münster, Germany
[c] Helmholtz-Institute Münster, IEK-12, Forschungszentrum Jülich GmbH, Corrensstraße 46, Münster 48149, Germany

ARTICLE INFO

Keywords:
Au(1 1 1)
Electrochemistry
Surface reconstruction
Surface dynamic
Ab initio simulations

ABSTRACT

We report in this communication, through *in situ* STM images correlated with time, and *ab initio* simulations of binding energies, how potential-induced surface reconstruction is formed on Au(1 1 1) single crystal in 0.1 M H_2SO_4. It was found that while the electrode potential after lifting the reconstructed surface is switched back to a more negative value than the potential of zero charge, the formation process of the reconstructed surface goes through two consecutive routes. In the more kinetically favorable step, and within a few minutes, the reconstructed surface follows three different lattice directions with a high proportion of *semi* zig-zag structures. However, by maintaining the negative applied potential, the surface reconstruction rearranges to a straighter reconstructed pattern in the second step, which is more energetically favorable.

1. Introduction

The development of electrochemical interface-based technologies like sensors, electrocatalysts, and storage systems, depends on the detailed structures of the atoms on the surface of the active substrates. In this regard, a deep understanding of the surfaces structural properties, especially in model systems of low-index metal electrodes play an essential role in defining the surface reactivity [1]. A clean surface of Au reconstructs by altering the position of the surface atoms to minimize the surface energy. In the case of Au(1 1 1), the reconstructed surface contains of a 4 % compression of the top layer in one of the three [1 1 0] directions. Proven first by *ex situ* electron diffraction experiments [2,3], the excess gold atoms create a pattern in which every 23rd surface atom to be in line with the underlying bulk ($\sqrt{3} \times 22$) [4]. The resulting straight ridges are features of a clean reconstructed Au(1 1 1) surface representing the most energetically favorable configuration (see Fig. 1a). More information on the properties of the reconstructed surface and its stability under electrochemical conditions can be found in the work of Kolb [4].

Experimental observation is that the application of an electrode potential sufficiently negative of the potential of zero charge (pzc) causes large portions of the surface to reconstruct within seconds or minutes [5]. It is proven experimentally that the reconstructed surface of Au(1 1 1) exhibits electrochemical properties that are different from unreconstructed ones. This can be reflected in their pzc values which are + 0.32 V and + 0.23 V vs saturated calomel electrode (SCE) for ($\sqrt{3} \times 22$) and (1×1), respectively [3]. Furthermore, theoretical investigations prove that the local distribution of atomic-level surface reconstruction shows slight reactivity variation across different surface sites [6].

A wide variety of structure-sensitive *in situ* techniques have been developed to investigate the physical and chemical properties of the reconstructed surface [6–9], among which *in situ* scanning tunneling microscopy (*in situ* STM) plays a significant role in advancing our knowledge about surface feature properties and electrochemical behavior with atomic resolution [7,10–13]. Kibler *et al.* used a combinational approach of *in situ* STM and hydrogen evolution reaction (HER) on Au(1 1 1) to monitor the structural changes on the surface. It was found in this study that the process of potential-induced surface reconstruction is much faster for the potential 0.415 than 0.115 V vs RHE. According to the authors, this observation might be due to the difference relative to the pzc, and the influence of anions covering the surface and increasing the mobility of surface atoms. This work also compares the potential-induced surface reconstruction at 0.415 and 0.115 V vs RHE after a long waiting time, observing a slight variation in the surface structures between these two potentials [14]. In a similar work to Kibler

* Corresponding author.
E-mail address: b.masoud@fz-juelich.de (M. Baghernejad).

https://doi.org/10.1016/j.elecom.2022.107332
Received 27 April 2022; Received in revised form 19 July 2022; Accepted 21 July 2022
Available online 25 July 2022

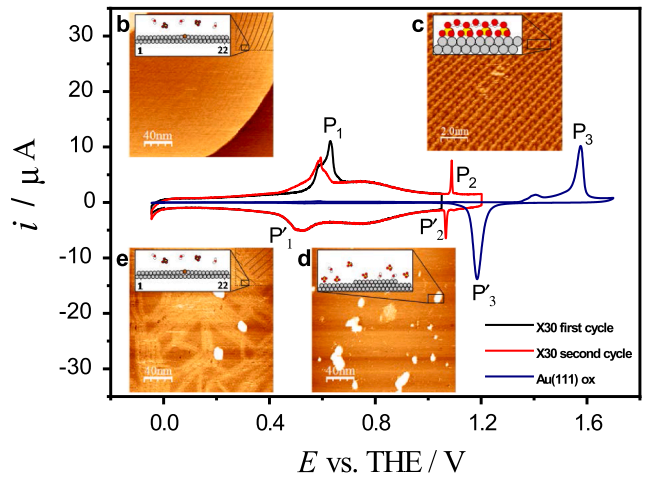

Fig. 1. (a) CV (scan rate 20 mV s^{-1}) and constant potential *in situ* STM images of Au(1 1 1)/H_2SO_4 at different potential regions. The peak pairs P_1/P'_1, P_2/P'_2, and P_3/P'_3 in the CV correspond to lifting of the reconstructed surface, sulfate ordered adsorption and Au(1 1 1) surface oxidation. *In situ* STM images show (b) reconstructed pattern at 0.0 V, scale bar 40 nm, (c) adsorbed sulfate ion ordered pattern at 1.2 V, scale bar 2 nm, (d) Au island formation due to the surface reconstruction lift-up at 0.8 V, scale bar 40 nm, and (e) electrode potential-induced reconstruction formation at 0.0 V, scale bar 40 nm. Inset cartoons are for illustrative purposes. The vertical dash lines show the pzc values for the reconstructed (red) and the unreconstructed (blue) surfaces.

et al. [14], Hermann *et al.* investigated the potential-induced surface reconstruction kinetics at potentials of −0.3 and −0.6 V vs mercury sulfate electrode (MSE) by probing HER on Au(1 1 1) surface. The HER activity in both potentials decays continuously over time as a result of potential-induced reconstruction. However, the HER activity decay is much faster in the more positive potential because at the potentials close to the lifting of the reconstruction, the reconstructed structures appear more rapidly. Also, at more negative potentials, the surface structure is dominated more by straight rows, while the herringbone structures are prominent at the positive potentials [15].

In this work, we present a voltammetric and *in situ* STM investigation of the potential-triggered reconstructed Au(1 1 1) surface in 0.1 M H_2SO_4. We demonstrate how inducing a constant electrode potential lower than pzc influences different energy states corresponding to different surface structures on the Au(1 1 1) surface at different time scales. Different to the work by Kibler *et al.* [14] and Hermann *et al.* [15], our observations showed a transition between different structures at a specific potential and after a certain waiting time. To the best of our knowledge, the exact dynamics and kinetics of the potential-triggered transition of unreconstructed to reconstructed surface of Au(1 1 1) employing sequential *in situ* STM images are not systematically established. Aided by *ab initio* calculations, we confirm that a *semi* zig-zag configuration of the reconstructed layer is higher in energy than a straight configuration, which supports our observation that reconstruction begins with disordered zig-zag conformations, but in time, reorders into straight rows. In other words, in this report, we show that even after reconstruction forms, the surface is still active. This new information has important consequences for our fundamental understanding of surface dynamics in wide range of disciplines, including condensed matter physics, surface technologies, and material science.

2. Experimental details

2.1. Chemicals and glassware

A 0.1 M solution of sulfuric acid (H_2SO_4, 98 %, Merck, suprapure) in Milli-Q water was prepared as the electrolyte for electrochemical experiments. Milli-Q water has resistivity higher than 18.2 MΩ cm and contains less than 2 parts per billion of total organic carbon. Argon gas was bubbled through the solution to remove oxygen. All the glassware and *in situ* STM cell compartments were cleaned by overnight soaking in piranha acid solution.

2.2. Cyclic voltammetry

A three-electrode cell with a half-bead Au(1 1 1) as the working electrode, Pt counter electrode and trapped-hydrogen reference electrode (THE) was used for cyclic voltammetry measurements. The THE was employed for this measurement is a Pt wire inside a glass tube bubbled with hydrogen in the cell and stopped bubbling during the measurement. The THE reference electrode is inserted in the electrolyte solution of the measurement. Therefore, considering the technical aspects of THE electrode in our specific system, there is no meaningful difference in the potential values between reference hydrogen electrode (RHE) and THE. An Autolab potentiostat PGSTAT302 N was used for controlled potentiometric measurements. No galvanostatic cycling was performed. Prior to experiments, the Au(1 1 1) electrode was annealed to red-hot temperature in a butane flame and cooled in an argon gas atmosphere. Contact with the solution (immersion) was made under potential control at 0.0 V vs THE in the hanging meniscus configuration.

2.3. In situ STM

In situ STM experiments were carried out with PicoPlus 5500 SPM system (Agilent Technologies, Inc.) equipped with an STM scanner (10 μm scanning range). A half-bead Au(1 1 1) single crystal was employed as a sample with Pt wires as pseudo-reference and counter electrodes. Prior to the measurements, the half-bead crystal was annealed in a constant butane flame at a slightly red color for 30 min and then cooled to room temperature in an argon gas atmosphere. A lab-build *in situ* STM cell, which was filled with the electrolyte under potential control, was used in all the *in situ* STM measurements.

Tungsten (Goodfellow, 0.25 mm in diameter, 99.999 %) tips were prepared with DC etching in 2 M KOH. This was done by vertically centering a tungsten wire inside a ring with a formed lamella (a thin film of liquid in the ring) beforehand. The optimum voltage for the etching of the tungsten tips was 2.7 V. The tips were then coated with polyethylene (PE). PE was melted with an iron and the tip was passed through the melted PE, leaving only the microscopic apex of the tungsten tip exposed. The tungsten tip was mounted a day before the measurements, and after assembling the *in situ* STM cell inside the scanner. the system was left untouched for 12 h to minimize the thermal and mechanical instabilities. However, a drift of a few nanometers per minute is observed in the acquired images.

2.4. *Ab initio* calculations

Ab initio calculations were performed to compare the energy of the *semi* zig-zag configuration with the straight rows. DFT calculations [16,17] were performed using the Vienna Ab-initio Simulation Package (VASP) computational package [18,19]. Spin polarization was activated. Calculations were done using the Perdew-Burke-Ernzerhof (PBE) generalized-gradient approximation [20]. The projected augmented wave (PAW) pseudopotential [20,21] of Au was employed in the calculation. Plane-wave cutoff was fixed at 520 eV. The Brillouin sampling was performed using Monkhorst-Pack grids with a *k*-grid of 4 × 3 × 1 which is found to be sufficient after testing the convergence of the energy with respect to size of the mesh. The model was a 4 × 6 supercell having 4 layers of Au atoms where only the top 2 layers are optimized while the bottom 2 layers remain fixed in their bulk position. The periodic images of the slab were separated by 20 Å vacuum. A climbing nudged elastic band (c-NEB) was also performed to calculate the value of the activation energy between the straight and zig-zag configurations. Three images between these two configurations are considered in this

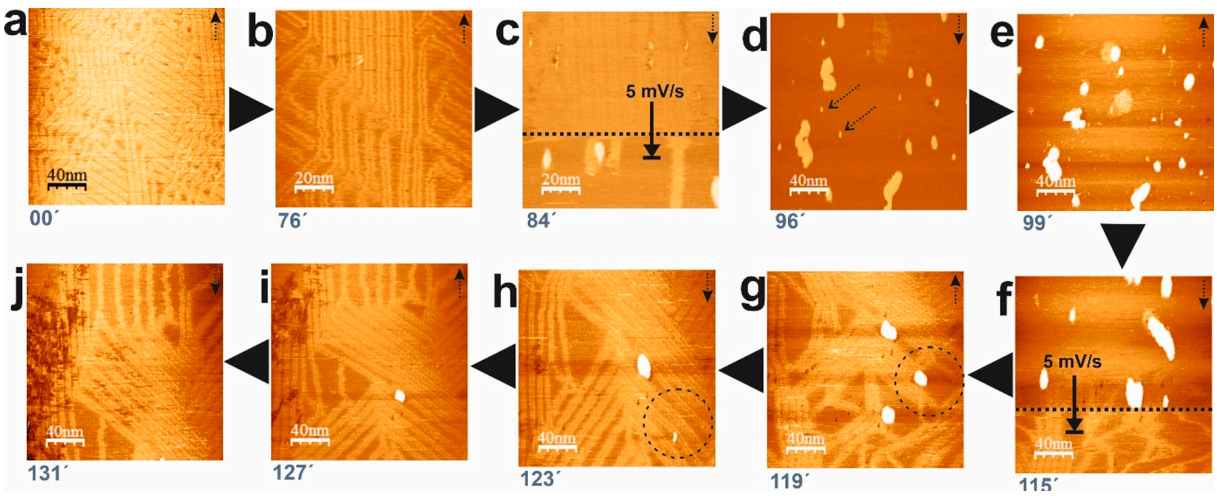

Fig. 2. Sequence of *in situ* STM images for Au(1 1 1) in 0.1 M H_2SO_4. (a) and (b) freshly thermally prepared reconstructed surface preserved at 0.0 V; (c) sweeping the potential from 0.0 to 0.8 V with the rate of 5 mV s^{-1} (dash line is the starting point to scan the potential from 0.0 V to 0.8 V); (d) and (e) lifting up of the reconstructed surface at 0.8 V; (f) sweeping back the potential to 0.0 V with the rate of 5 mV s^{-1} (dash line is the starting point to scan the potential from 0.0 V to 0.8 V); and (g), (h), (i), and (j) potential-induced formation of the reconstruction surface at 0.0 V. The scale bar of each image is given in the bottom left corner of each image. The scan direction is illustrated with an arrow in the upper right corner of the images. The time duration of the acquired images referenced in Fig. 2a for time zero and is displayed below each image. The tunneling current was kept for all the images at 0.9 nA and the tip-substrate bias potential at 0.2 V.

study. Atomic simulation environment (ASE) [22] was used to generate the Au slab, and Visualization for Electronic and Structural Analysis (VESTA) [23] was used for the visualizations.

3. Results

3.1. Cyclic voltammetry

A representative CV, with a 20 mV s^{-1} potential scan rate, of the freshly annealed Au(1 1 1) electrode in 0.1 M H_2SO_4 was shown in Fig. 1. The immersion potential of the sample in the electrolyte was kept at $E =$ 0.0 V vs THE. This potential was chosen because the reconstructed surface remained stable in this region of the CV [24]. Three pairs of peaks were seen in this voltammogram, denoted as P_1/P'_1, P_2/P'_2, and P_3/P'_3. These peaks corresponded to the lifting of the reconstructed surface and adsorption of the sulfate ions, ordered sulfate phase formation, and oxidation of Au surface, respectively. During the positive potential scan, a sharp peak, P_1, assigned to the lifting up of the surface reconstruction, appeared at $E > 0.4$ V. The corresponding reduction peak system, P'_1, was observed during the reverse potential scan in the potential range 0.40 V $< E <$ 0.50 V. The second pair, P_2/P'_2, corresponds to the transition of sulfate ion adsorption from disordered to ordered and vice versa. The disordered adsorption of sulfate started at the potentials where the reconstructed layer was lifted (broad peak in the voltammogram between P_1 and P_2). The peak pair, P_3/P'_3, in the CV represented Au(1 1 1) surface oxidation and reduction, respectively.

As shown in the CV in Fig. 1a, the P_1 peak looked different in cycles one to two. This was, in part, due to the lifting up of the reconstructed surface preserved in the first cycle from thermal annealing. In the second cycle (scan rate still 20 mV s^{-1}) a complete potential-induced formation of the reconstructed surface was not possible (corresponding P'_1 peak). Therefore, the P_1 peak was distorted in the second cycle compared to the first one. Furthermore, with increasing defect density after surface oxidation and reduction (P_3/P'_3), the P_1 peak was shifted towards more negative potentials. According to Kolb, the ($\sqrt{3} \times 22$) to (1 × 1) is a nucleation-and-growth process which starts at the defects [4]. Therefore, a defect-rich surface after the surface oxidation facilitates the nucleation rate and causes a shift in the P_1 peak in the second cycle. Also, it was suggested in this paper that the potential-induced reconstruction follows the same nucleation-and-growth process which may result in faster kinetics in a defect-rich Au(1 1 1) surface.

3.2. In situ STM study of thermally-induced reconstruction

Fig. 1b showed a freshly made thermally-induced surface reconstruction of Au(1 1 1) preserved in 0.1 M H_2SO_4 and at the immersion electrode potential of 0.0 V vs THE (see Figure SI1 in the *Supporting Information* for more detailed images). As shown in Fig. 1d, the reconstruction was lifted at more positive potentials by specific adsorption of sulfate ions and the formation of unreconstructed (1 × 1) surfaces. This was indicated by the anodic current peaks around 0.63 V vs THE for Au (1 1 1) in Fig. 1a.

Fig. 1c demonstrated the ordered sulfate ion adsorption following P_2, at potentials above ca. 1.1 V. It was proposed by Edens *et al.* [25] that the sulfate ion structure on the Au(1 1 1) surface is formed of simultaneous hydronium ions coadsorption to diminish the coulombic repulsions between adjacent sulfate ions. It is important to mention that the adsorption of sulfate ions on the surface starts at the potentials around P_1 in the positive direction, and at electrode potentials more positive than 1.1 V vs THE adsorbed sulfate ions start to form ordered domains as shown in Fig. 1c and Figure SI2. More information on properties and different models of sulfate adsorption on Au(1 1 1) electrode can be found elsewhere [26].

Fig. 1d depicted the transition of the reconstructed ($\sqrt{3} \times 22$) surface to unreconstructed (1 × 1) by forming Au islands on the surface. As mentioned earlier, since the reconstructed surface was slightly more stable than the unreconstructed surface, a relatively small difference in adsorption energies triggered by the electrode potential was sufficient to lift the reconstructed layer. This was a semi-reversible process in which, in order to obtain the reconstructed surface again, the electrode potential had to be switched to the region between P'_1 and the immersion potential of 0.0 V vs THE (see Fig. 1e).

3.3. Potential-induced reconstruction of Au(1 1 1)

As shown in Fig. 1, upon sulfate ions adsorption (around the pzc potential), the surface undergoes a structural transition to (1 × 1). Hermann *et al.* reported pzc values −0.09 and −018 V vs MSE for the reconstructed and the unreconstructed surfaces, respectively [15]. Calibrating these values in our CV measurements shows pzc values of 0.75 and 0.66 V vs THE for the reconstructed and the unreconstructed surfaces, respectively. The *in situ* STM images (Fig. 1d and e) for Au(1 1 1)-($\sqrt{3} \times 22$) and -(1 × 1) at selected potentials enabled us to monitor the

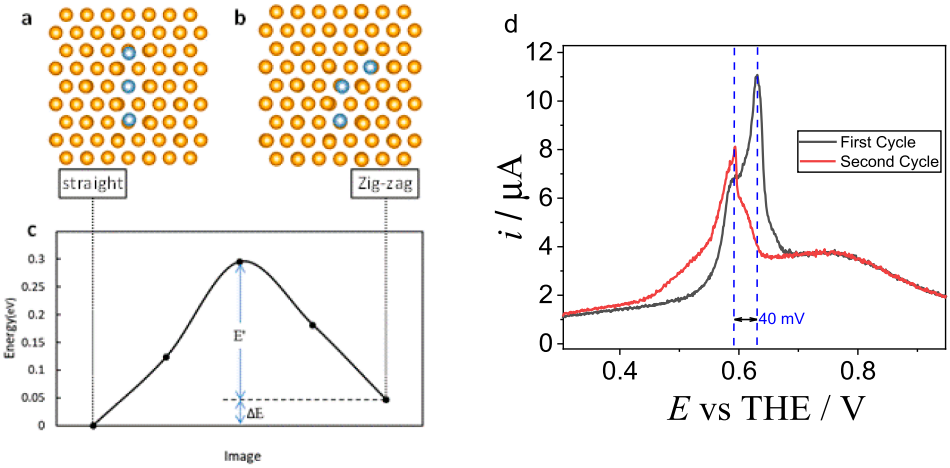

Fig. 3. *Ab initio* model for calculating relaxed energy for (a) straight and (b) zig-zag Au adlayer configuration; (c) Energy curve based on c-NEB calculation between reconstructed configurations. (d) CV peaks for the first and second cycle of the ($\sqrt{3} \times 22$) to (1 × 1) transition from Fig. 1.

change in the surface structure during a potential sweep, and hence to establish the structural features of the Au(1 1 1) surfaces in various electrode potentials, and at specific times.

By way of determining a detailed correlation of structural and electrochemical data, it should be noted that, unlike the transition of ($\sqrt{3} \times 22$) to (1 × 1), the potential-induced reconstruction of the Au(1 1 1) surface had much slower kinetics. This was mainly due to the metastable nature of the unreconstructed surface that needs activation energy to form a reconstructed surface. The activation energy under electrochemical conditions for this transition is substantial because it is involved with bond breaking and gold atom migration on the surface [4].

Fig. 2 showed a sequence of time evolution *in situ* STM images by switching the potential between the reconstructed (0.0 V vs THE) and the unreconstructed (0.8 V vs THE) surfaces of Au(1 1 1) in 0.1 M H_2SO_4 electrolyte. Fig. 2a and b showed the *in situ* STM images of thermally prepared reconstruction (similar to Fig. 1b). Sweeping the potential with 5 mV s^{-1} scan rate from 0.0 V to 0.8 V leads to immediate lifting of the reconstruction, as shown in Fig. 2c. As clearly seen in Fig. 1d, the immediate lifting of the reconstruction created monoatomic high Au islands from the extra 4 % of atoms on the surface (see Figure SI3), with sizes ranging from a few Au atoms to tens of nanometers. However, the surface remained dynamic and small islands joined the bigger ones on the surface by time. Two examples of these islands were shown in Fig. 2d in which they disappeared in Fig. 2e within ca. 3 min. Although the removal of the reconstructed surface occurred quickly, the reverse process was relatively slow. Fig. 2f showed an *in situ* STM image while sweeping the potential back to 0.0 V with the scan rate of 5 mV s^{-1}. After sweeping the potential back, a series of *in situ* STM images were shown at constant 0.0 V in Fig. 2g-j, which depicted island dissolution and potential-induced surface reconstruction formation within ca. 30 min. Looking closely at the islands as the main source for the reconstructed surface, a simultaneous dynamic shrinking of the islands and re-patterning of the reconstructed surface was observed. The former was in agreement with previous reports, however the latter observation at a longer timescale has not been reported, to our best knowledge. According to Kolb *et al.*, potential-induced reconstruction of the Au(1 1 1) surface, unlike the thermally heated reconstruction, is no longer aligned in only one direction but runs a *semi* zig-zag in all three main crystallographic directions of the Au(1 1 1) substrate [4]. However, what was observed in Fig. 2f-j, was a two-step process. At first, and within 5 min, similar to previous reports, the formation of the reconstructed surface started in all three main crystallographic directions of the Au(1 1 1) substrate. Also, the rims of the monoatomic high Au islands served as nucleation centers for the (1 × 1)-($\sqrt{3} \times 22$) structural transition. In the second step, the initially formed reconstructed surface underwent rearrangement and formed a more energetically stable reconstructed surface with more straight patterns rather than the *semi* zig-zag structures. One example of such a transition is depicted in Fig. 2g and f with a dashed circle corresponding to the same area on the Au(1 1 1) surface.

3.4. Two-step reconstruction and ab initio calculation

Another important parameter that played a role in defining the two-step process was the transition kinetics. A kinetically faster forming zig-zag structure presented within a few minutes after sweeping back the potential to 0.0 V. However, the more thermodynamically stable form of the reconstruction appeared as the electrode potential was held at 0.0 V and while the monoatomic high Au islands were disappearing.

Fig. 3a and 3b depicted cartoons of the models compared in this study. In Fig. 3a, the Au adatoms, colored silver, were aligned in a row atop the Au(1 1 1) sublayer, colored gold; in Fig. 3b, by contrast, the Au adatoms were in a zig-zag orientation. The calculated energy difference between the relaxed systems was 47 meV that is in good agreement with the experimental results of- 40 mV calculated from the ($\sqrt{3} \times 22$) to (1 × 1) transition peaks in Fig. 3d. This comparison made based on the fact that thermally-annealed surface forms dominantly straighter configuration of ($\sqrt{3} \times 22$) than potential-induced one in the time scale of the measurements. Fig. 3c depicts the energy profile of the two configurations. The activation energy, E*, according to the c-NEB calculation, was found to be 295 meV which is large enough for the zig-zag to form and remain momentarily.

4. Conclusion

This study showed an *in situ* STM investigation of Au(1 1 1) surface for potential-induced surface reconstruction in sulfuric acid electrolyte. It was found that a potential-induced surface reconstruction forms two surface patterns of straight and *semi* zig-zag configurations. The energy difference between the two configurations in Fig. 3c explained why the initial step during Au(1 1 1) reconstruction permits random *semi* zig-zag configurations, observed in Fig. 2a and b, for the initial ca. 3 min. Yet when sufficiently negative potentials were held for sufficiently long period of time, the surface achieved the lower-energy straight configuration. This two-step route has not been reported previously. We expect that it is always present, but the transience of the first step means the second step dominates after c. 3 min.

CRediT authorship contribution statement

Joseph Hamill: Methodology, Formal analysis, Investigation, Writing – original draft, Writing – review & editing, Funding acquisition. **Kazem Zhour:** Methodology, Investigation, Data curation, Writing – original draft, Writing – review & editing. **Diddo Diddens:** Methodology, Investigation, Data curation, Writing – original draft, Writing – review & editing. **Masoud Baghernejad:** Conceptualization, Methodology, Investigation, Data curation, Writing – original draft, Writing – review & editing, Supervision, Project administration, Funding acquisition.

Declaration of Competing Interest

The authors declare that they have no known competing financial interests or personal relationships that could have appeared to influence the work reported in this paper.

Data availability

Data will be made available on request.

Acknowledgment

Financial support from the German Federal Ministry for Education and Research within the project EFoBatt (grant number 13XP5129) is gratefully acknowledged. The work of Joseph Hamill has received funding from the European Union's Horizon 2020 research and innovation programme under the Marie Skłodowska-Curie grant agreement No 884741.

Appendix A. Supplementary material

Supplementary data to this article can be found online at https://doi.org/10.1016/j.elecom.2022.107332.

References

[1] L.A. Kibler, Preparation and characterization of noble metal single crystal electrode surfaces, ISE, Barcelona, 2003.
[2] G.L.M.S. Zei, D.M. Kolb, On the stability of reconstructed gold surfaces in an electrochemical Cell, Surf. Sci. 221 (1989) 23.
[3] D.M. Kolb, J. Schneider, Surface reconstruction in electrochemistry: Au(100−(5 × 20), Au(111)−(1 × 23) and Au(110)−(1 × 2), Electrochim. Acta 31 (1986) 929–936.
[4] D. Kolb, Reconstruction phenomena at metal-electrolyte interfaces, Prog. Surf. Sci. 51 (2) (1996) 109–173.
[5] J. Schneider, D.M. Kolb, Potential-induced surface reconstruction of Au(100), Surf. Sci. 193 (3) (1988) 579–592.
[6] F. Hanke, J. Björk, Structure and local reactivity of the Au(111) surface reconstruction, Phys. Rev. B 87 (2013), 235422.
[7] G. Nagy, T. Wandlowski, Double layer properties of Au(111)/H_2SO_4 (Cl) + Cu^{2+} from distance tunneling spectroscopy, Langmuir 19 (2003) 10271–10280.
[8] J.M. Artés, I. Díez-Pérez, F. Sanz, P. Gorostiza, Direct measurement of electron transfer distance decay constants of single redox proteins by electrochemical tunneling spectroscopy, ACS Nano 5 (3) (2011) 2060–2066.
[9] S.L. Yau, Y.H. Lee, C.Z. Chang, L.J. Fan, Y.W. Yang, W.P. Dow, Structures of aniline and polyaniline molecules adsorbed on Au(111) electrode: as probed by in situ STM, ex situ XPS, and NEXAFS, J. Phys. Chem. C 113 (2009) 13758–13764.
[10] D.M. Kolb, An atomistic view of electrochemistry, Surf. Sci. 500 (1-3) (2002) 722–740.
[11] N.J. Tao, C.Z. Li, H.X. He, Scanning tunneling microscopy applications in electrochemistry—beyond imaging, J. Electroanal. Chem. 492 (2) (2000) 81–93.
[12] H.Y. Nie, W. Mizutani, H. Tokumoto, Au(111) reconstruction observed by atomic force microscopy with lateral force detection, Surf. Sci. Lett. 311 (1-2) (1994) L649–L654.
[13] Y. Hasegawa, P.h. Avouris, Manipulation of the reconstruction of the Au(111) surface with the STM, Science 258 (5089) (1992) 1763–1765.
[14] L.A. Kibler, J.M. Hermann, A. Abdelrahman, A.A. El-Aziz, T. Jacob, New insights on hydrogen evolution at Au single crystal electrodes, Curr. Opin. Electrochem. 9 (2018) 265–270.
[15] J.M. Hermann, A. Abdelrahman, T. Jacob, L.A. Kibler, Potential-dependent reconstruction kinetics probed by HER on Au(111) electrodes, Electrochim. Acta 347 (2020), 136287.
[16] W. Kohn, L.J. Sham, Self-consistent equations including exchange and correlation effects, Phys. Rev. 140 (4A) (1965) A1133–A1138.
[17] P. Hohenberg, W. Kohn, Inhomogeneous electron gas, Phys. Rev. 136 (3B) (1964) B864–B871.
[18] G. Kresse, J. Hafner, Ab initio molecular dynamics for liquid metals, Phys. Rev. B 47 (1) (1993) 558–561.
[19] G. Kresse, J. Furthmüller, Efficient iterative schemes for ab initio total-energy calculations using a plane-wave basis set, Phys. Rev. B 54 (16) (1996) 11169–11186.
[20] J.P. Perdew, K. Burke, M. Ernzerhof, Generalized gradient approximation made simple, Phys. Rev. Lett. 77 (18) (1996) 3865–3868.
[21] G. Kresse, D. Joubert, From ultrasoft pseudopotentials to the projector augmented-wave method, Phys. Rev. B 59 (3) (1999) 1758–1775.
[22] A. Hjorth Larsen, J. Jørgen Mortensen, J. Blomqvist, I.E. Castelli, R. Christensen, M. Dułak, J. Friis, M.N. Groves, B. Hammer, C. Hargus, E.D. Hermes, P.C. Jennings, P. Bjerre Jensen, J. Kermode, J.R. Kitchin, E. Leonhard Kolsbjerg, J. Kubal, K. Kaasbjerg, S. Lysgaard, J. Bergmann Maronsson, T. Maxson, T. Olsen, L. Pastewka, A. Peterson, C. Rostgaard, J. Schiøtz, O. Schütt, M. Strange, K. S. Thygesen, T. Vegge, L. Vilhelmsen, M. Walter, Z. Zeng, K.W. Jacobsen, The atomic simulation environment—a python library for working with atoms, J. Phys.: Condens. Matter 29 (27) (2017) 273002, https://doi.org/10.1088/1361-648X/aa680e.
[23] K. Momma, F. Izumi, VESTA 3 for three-dimensional visualization of crystal, volumetric and morphology data, J. Appl. Crystallogr. 44 (2011) 1272–1276.
[24] O.M. Magnussen, J. Hotlos, R.J. Behm, N. Batina, D.M. Kolb, An in-situ scanning tunneling microscopy study of electrochemically induced "Hex" ↔ (1 × 1) transitions on Au(100) electrodes, Surf. Sci. 296 (3) (1993) 310–332.
[25] G.J. Edens, X. Gao, M.J. Weaver, The adsorption of sulfate on gold(111) in acidic aqueous media: adlayer structural inferences from infrared spectroscopy and scanning tunneling microscope, J. Electroanal. Chem. 375 (1994) 357–366.
[26] K.-I. Ataka, M. Osawa, In situ infrared study of water−sulfate coadsorption on gold (111) in sulfuric acid solutions, Langmuir 14 (4) (1998) 951–959.